Identification of Active Sites of Biomolecules II: Saccharide and Transition Metal Ion in Aqueous Solution

Orkid Coskuner,*,†,‡ Denis E. Bergeron,† Luis Rincon,†,§ Jeffrey W. Hudgens,* and Carlos A. Gonzalez*,†

Computational Chemistry Group, Physical and Chemical Properties Division, National Institute of Standards and Technology, 100 Bureau Drive, Mail Stop 8380, Gaithersburg, Maryland 20899, Computational Materials Science Center, George Mason University, Research I, Fairfax, Virginia 22030, and Departamento de Química, Universidad de los Andes, Mérida-5101, Venezuela

Received: June 30, 2008; Revised Manuscript Received: November 28, 2008

We discuss the coordination mechanism of Fe^{III} and methyl-α-mannopyranoside in aqueous solution using a recently presented integrated approach comprising ab initio electronic structure calculations, molecular dynamics simulations, and mass spectrometric measurements. First principles Car−Parrinello molecular dynamics (CPMD) simulations find that a single Fe^{III} ion interacts with specific hydroxyl groups of the saccharide in aqueous solution. Specifically, we find that one Fe^{III} ion complexed to methyl-α-mannopyranoside also associates with two water molecules. These simulations are in accord with electrospray ionization mass spectrometry measurements involving guided ion beam hydration measurements, which reveal an optimal coordination number of four about the Fe^{III} ion. CPMD simulations identified specific intramolecular and intermolecular hydrogen bonding interactions that have an impact on the conformation of the saccharide and on the coordination with Fe^{III}; in contrast, classical molecular dynamics simulations were insensitive to these effects. This study illustrates the strength of ab initio molecular dynamics simulations, chemical reactivity calculations, and natural partial charge analysis coupled with mass spectrometric measurements in identifying the active sites of biomolecules toward ligands and for studying the complexation and coordination chemistry associated with substrate and ligand interactions relevant to the design of biochemical syntheses, drugs, and biomarkers in medicine.

I. Introduction

The development of biological inorganic chemistry that studies complexes of metal ions and biomolecules is driven by several factors, including attempts to reveal the interplay between metal ions and biomolecules, efforts to understand the metabolism and transport of metal−organic complexes, development of biometallic drugs and biomarkers, the utilization of powerful spectrometric tools allowing studies of metal−organic structures, and the use of macromolecular engineering techniques to develop novel structures relevant in biochemistry, medicine, and nanobiotechnology. Furthermore, the relevance of metal ions in the functions and health of living organisms is well documented. In spite of all the progress made, we are still only on the brink of understanding biometallic systems and their coordination chemistry in solution.

Solvent effects present further difficulties in studying biometallic compounds. However, these effects must be accounted, given that a significant fraction of the human body is composed of water and most relevant biomolecular and biometallic reactions of physiological and technological relevance are to some extent solvent mediated. Water gives rise to hydrophobic interactions[1,2] that stabilize the core of globular proteins,[3] is thought to weaken and diminish electrostatic interactions in many biomolecules, and has the role of filling internal cavities of proteins,[4] oligosaccharides,[5−7] and nucleic acids.[8] Moreover, water molecules can be tightly associated with the surfaces of biomolecules, occupying certain more or less well-defined positions and interacting with surrounding water molecules through hydrogen bonds.[9] Even though much effort has been expended on studies of liquid water and aqueous-phase biomolecules, the role of water in the coordination chemistry of biometallic compounds remains poorly understood.

Experimental measurements utilizing extended X-ray absorption fine structure, X-ray, and neutron diffraction are useful to obtain structural information, and nuclear magnetic resonance, infrared (IR), and Raman spectroscopies are used for investigating the structure and dynamical properties of biomolecules in aqueous solution.[10] Interpreting the results from these experimental techniques can be immensely challenging, and in particular, it is difficult to produce direct measurements of the local electronic structure of the reaction medium associated with the fast dynamics of biometallic systems. Limited information can be found in X-ray analysis, which has been used to determine pair correlation functions.[10−12] However, these functions are usually spherically averaged, and thus, details of structuring in aqueous biomolecule solutions are difficult to predict accurately since important information linked to anisotropic and asymmetric characters of the system are lost.[11,12]

Challenges to computational studies of biometallic systems are associated with relatively large molecular sizes, long timescales, and a large number of degrees of freedom. Static first principles calculations in the gas phase and in aqueous solution using continuum models for water have been applied extensively for predicting the structure and function of aqueous biomolecules

* Corresponding author. E-mail: orkid.coskuner@nist.gov (O.C.), jeffrey.hudgens@nist.gov (J.W.H.), and carlos.gonzalez@nist.gov (C.A.G.).
† National Institute of Standards and Technology.
‡ George Mason University.
§ Universidad de los Andes.

10.1021/jp805747f CCC: $40.75
Published on Web 02/23/2009

and biometallic compounds.[13−16] Even though these ab initio calculations are relatively efficient in terms of computational time, static gas phase calculations cannot capture the impact of the dynamics nor the effect of water on the predicted structures of the compounds of interest. Continuum water calculations ignore intermolecular hydrogen bonding interactions, which can have a large impact on the predicted structure and conformation of most biomolecules and biometallic compounds. Classical molecular dynamics (CMD) and Monte Carlo (MC) simulations are the most widely used computational tools to study biomolecules and biometallic systems in aqueous solution.[17−21] Even though classical simulations have been useful to a great extent, the accuracy of these simulations depends on the quality of the chosen force field parameters, and these simulations ignore the impact of quantum effects in predicting the structure and function of biomolecules and biometallic systems.

In a recent study, we presented a novel strategy that employed theoretical calculations, molecular dynamics simulations, and mass spectrometric experiments to identify the active sites of methyl-α-mannopyranoside (M) toward a transition metal ion in the gas phase.[22] Our density functional theory (DFT) chemical reactivity index calculations and Car−Parrinello molecular dynamics (CPMD) simulations showed that Fe^{III} interacts with specific hydroxyl oxygen atoms of the carbohydrate, and these predictions were shown to be in accord with our mass spectrometric measurements.[22] Furthermore, our CPMD simulations indicated that the specific conformational preference of the glycosidic linkage of M in the gas phase is influenced by intramolecular hydrogen bonding interactions. In contrast, our classical molecular dynamics (CMD) simulations using OPLS-AA and UFF parameters for the carbohydrate and the metal ion, respectively,[36,37] converged to structures that are discordant with the mass spectrometry data, evidence that these CMD simulations are insensitive to these effects. This comparison demonstrates the importance of chemical reactivity calculations and CPMD simulations for predicting the active sites of the biomolecule toward metal ions.[22]

In the present work, we apply DFT chemical reactivity index calculations and CPMD simulations to identify the active sites of M toward Fe^{III} in water. We examine the coordination mechanism and the impact of both Fe^{III} and solvent on the predicted conformation of the carbohydrate. Results are then compared to those obtained via CMD simulations. We find that a single Fe^{III} ion, to which two water molecules are bound ($Fe(H_2O)_2^{3+}$), coordinates to specific hydroxyl oxygen atoms of the carbohydrate, and a second Fe^{III} ion forms an octahedral $Fe(H_2O)_6^{3+}$ complex in the second solvation shell. Specifically, our ab initio studies suggest that intra- and intermolecular hydrogen bonding interactions stabilize the $g+$ (clockwise) orientation of the glycosidic linkage of the metal−carbohydrate complex over its t (trans) and g (anticlockwise) orientations and that hydrogen bonding interactions affect the coordination of the carbohydrate to the metal ion. In contrast, CMD simulations converged to structures that do not indicate coordination between the metal ion and the biomolecule.

Predictions of our theoretical studies are supported by ion beam hydration experiments conducted within a triple-quadrupole mass spectrometer. The use of mass spectrometric techniques to investigate hydration behavior is well-documented, and past studies have enabled the observation of magic number distributions (so that specific hydration shell cut-offs could be established), and even precise determinations of enthalpies of hydration for selected ionic analytes.[23−29] Many early studies involved hydration at molecular or metal centers,[23−26] but electrospray ionization (ESI) techniques have made possible the interrogation of biomolecules and metal−biomolecule systems.[27−29] The studies presented here treat the first two water molecule additions to the $[MFeCl_x]^+$ ($x = 1,2$) complexes, and we identify the threshold between chemical bond formation and hydrogen bond formation. This determination sheds light on the details of coordination in the complexes. The accord between the CPMD simulations and these experimental data is striking. We suggest that the integrated experimental and computational approach described herein and in ref 22 may be useful in the chemical description of a broad range of important biometallic systems in solution.

II. Methods

A. Car−Parrinello Molecular Dynamics Simulations. All CPMD simulations were performed with the NWCHEM program.[30,31] The Becke−Lee−Yang−Parr (BLYP) gradient corrected DFT functional was used along with Troullier-Martins pseudopotentials.[32,33a] The molecular orbitals were expanded in a plane wave basis set with a kinetic energy cutoff of 114 Ry. The time step for the simulation was set to 0.1 fs and the electronic mass was set to 900 au.

Hydrogen atoms were replaced by deuterium atoms as per standard procedures[33b−e] to allow larger time steps via CPMD simulations. A recent study by Chen et al. shows that the difference in water structure for H_2O and D_2O is very small at room temperature, proposing the difference to be within the noise of neutron scattering experiments.[33f,g] In addition, Hart et al. performed high energy X-ray measurements and computational simulations between 279 and 318 K, proposing that the quantum isotope effect is inversely proportional to increasing temperature.[33h] These findings indicate that the isotope effect is small around room temperature. Nevertheless, we would like to point out that this study does not include the isotope effect on aqueous carbohydrates around room temperature.

Simulations of M were performed with 58 water molecules in a cubic cell of lattice parameters of 16.6 Å. A homogeneous background charge was applied to compensate for ionic charge. Simulations for 80 ps were performed for M, MFe^{III}, and MFe^{III}_2 in aqueous solution (58 water molecules), and statistics were collected for the last 70 ps, respectively. To assess the effects of chosen number of water molecules on the simulated structures, a second set of simulations were performed using 92 water molecules (corresponding to a density of 0.998 g cm^{-3} for water). The structures obtained by these simulations differ from each other by 1.6%, indicating that the effects of additional water is small. Canonical ensemble simulations were performed with periodic boundary conditions at 300 K and at a pressure of 0.1 MPa using the Nose-Hover thermostat for controlling the temperature. Long-range interactions were treated with the Ewald sum method.[29]

B. Classical Molecular Dynamics Simulations. All classical MD simulations were performed using the NAMD program.[35] The OPLS-AA and UFF parameters were chosen for the carbohydrate and metal ion, respectively.[36,37] Our recent studies on methyl-α-mannopyranoside and methyl-β-mannopyranoside in aqueous solution using TIP3P, TIP4P, and TIP5P models for water showed that simulation results with the TIP5P model for water are closer to the results obtained via CPMD simulations.[6,7] Thus, we use the TIP5P potential function for water in this work to study the impact of water on the predicted conformation of the biometallic system.[1,2] Simulations for 50 ns were performed for M, MFe^{III}, and MFe^{III}_2 in aqueous solution and statistics were collected for the last 40 ns. For these

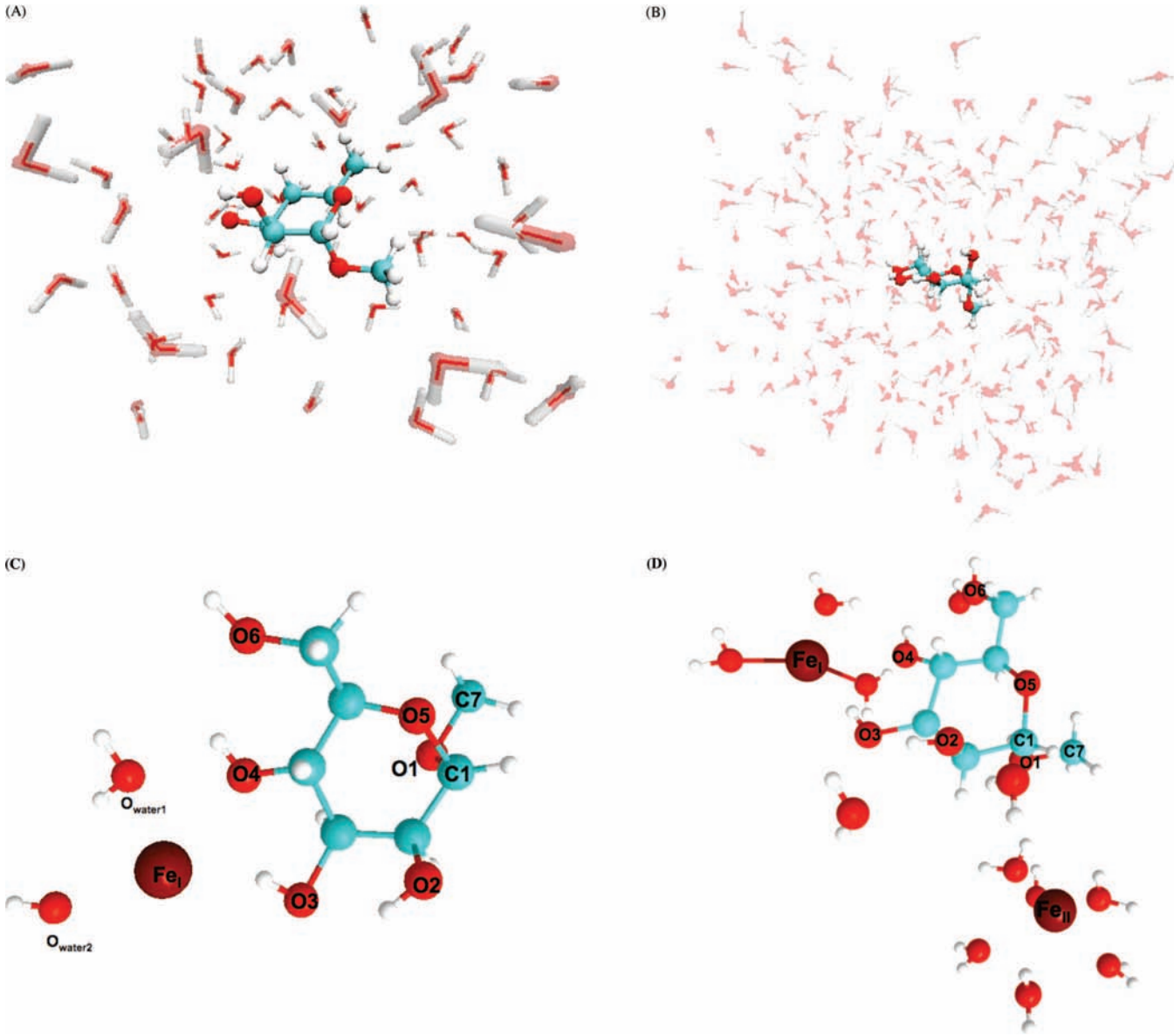

Figure 1. Methyl-α-D-mannopyranoside molecule in water (A) obtained from CPMD simulations, (B) obtained from CMD simulations, and its complexes with one and two Fe^{III} ions (C, D), obtained from CPMD simulations, with conventional numbering of specific atoms.

simulations, M was solvated in a cubic box containing 470 water molecules with a box length of 24.4 Å using periodic boundary conditions. A cutoff distance of 12 Å was used for solute and solvent long-range interactions and long-range electrostatic interactions were treated with the Ewald sum method.[34] These canonical ensemble simulations were coupled to an external bath at 300 K by Langevin dynamics.

C. Determination of the Conformational Preference of the Glycosidic Linkage. Figure 1 shows the structure of M with the numbering of specific heavy atoms. The glycosidic linkage, defined by the torsional angle φ = O5−C1−O1−C7, was varied from −180° to 180° to study the relative torsional energies. Encouraged by the success of our recent applications of the potential of mean force (PMF) method on carbohydrates and biometallic compounds using CPMD and CMD simulations,[6,16,17,22,38] we determined the PMF of the glycosidic linkage of M in aqueous solution and in the vicinity of Fe^{III} ions using eq 1.

$$\Delta G = -kT \ln Z \quad (1)$$

where Z is the probability of the torsional angle of the glycosidic linkage between −180° and 180° obtained via CPMD and classical MD simulations. For the CPMD simulations ($\lambda = 0 \rightarrow \lambda = 1$, where $\lambda = 0$ and $\lambda = 1$ are the initial and final state coupling parameters for the 20 windows defined in this work), the system was simulated for 60 ps for each window. To establish the adequacy and the convergence of PMF, calculated values were compared to those obtained for $\lambda = 1 \rightarrow \lambda = 0$. In addition, PMF values were compared with those obtained from 30, 40, and 50 ps simulations for each window. The standard deviation in PMF was computed utilizing results obtained from these different CPMD simulation times. For the classical MD simulations, each system was simulated for 600 ps for each window and the convergence was tested by comparing PMF values obtained for $\lambda = 0 \rightarrow \lambda = 1$ to those computed for $\lambda = 1 \rightarrow \lambda = 0$. PMFs were also compared with results obtained from 300, 400, and 500 ps classical simulations for each window. The standard deviation was calculated utilizing different classical MD simulation times. The standard deviations do not exhibit any definite trends and indicate that the systems are equilibrated and exhibit statistical fluctuations around the average PMF profile determined by CPMD and classical MD simulations, respectively.

TABLE 1: Calculated Chemical Reactivity Indices Based on Condensed Fukui Functions (f_i^{HOMO}): Methyl-α-D-mannopyranoside and Fe^{III} and Methyl-α-D-mannopyranoside in Water

atom	M	M:Fe^{III}
O2	0.18068	0.01602
O3	0.00107	0.00125
O6	0.00004	0.00022
O4	0.00412	0.00309
O5	0.00036	0.00092
O1	0.00165	0.00002

TABLE 2: Calculated Natural Partial Charges (NPA) for the Metal Ion and the Specific Carbohydrate Atoms Using the BLYP Method and 6-311+G(2d,p) Basis Set[a]

atom	M	M:Fe^{III}	M:Fe^{III}_2
O1	-0.58 ± 0.04	-0.57 ± 0.03	-0.59 ± 0.02
O2	-0.79 ± 0.02	-0.78 ± 0.02	-0.81 ± 0.03
O3	-0.77 ± 0.02	-0.73 ± 0.01	-0.71 ± 0.03
O4	-0.75 ± 0.04	-0.79 ± 0.02	-0.80 ± 0.02
O5	-0.56 ± 0.02	-0.62 ± 0.05	-0.61 ± 0.04
O6	-0.79 ± 0.03	-0.79 ± 0.02	-0.83 ± 0.02
Fe_I^{III}		0.72 ± 0.03	1.37 ± 0.04
Fe_{II}^{III}			1.11 ± 0.05

[a] Trajectories used in NPA calculations belong to the minimum energy configurations of the glycosidic linkage of the carbohydrate in water (including water molecules) obtained from CPMD simulations for aqueous methyl-α-D-mannopyranoside, methyl-α-D-mannopyranoside and Fe^{III} ion in water, and methyl-α-D-mannopyranoside and two Fe^{III} in water. Note that the ± are not uncertainties but give a range for the fluctuations around the equilibrium values. These fluctuations were determined via the time-dependent standard deviation method.

D. Chemical Reactivity Index. As in our previous work,[22] we employed chemical reactivity indices to identify chemically active sites on the substrate, M. The application of Fukui functions (FF) within the DFT formalism has been previously enumerated,[39−43] and we follow here the procedures outlined in this paper's prequel.[22] The methodology was implemented in the Gaussian 03 package,[44] and specific FF's were computed via single-point calculations on the geometries obtained from CPMD simulations; we employed the gradient corrected DFT PBE exchange-correlation functional,[45] using the 6−31G** basis (PBE/631G**//CPMD). The index, f_i^{HOMO} is a quantitative measure of the susceptibility of an atom, i, to electrophilic attack. We examined the relevant indices for the reactions: $M + nFe^{3+}$ (with $n = 0$ and 1) in water.

E. Experimental Method. Iron (III) chloride and methyl-α-D-mannopyrannoside were dissolved in methanol in a 1:5 ratio. Dilute solutions ($[FeCl_3] \approx 50\ \mu mol\ L^{-1}$) were introduced to a Micromass Quattro Micro-triple quadrupole instrument[31] via direct infusion at $10\ \mu L\ min^{-1}$. The electrospray ion source conditions were tuned to maximize signal intensity for the complex of interest and were similar to those employed during our recent collision induced dissociation (CID) studies.[22] To probe the interaction of $[MFeCl_x]^+$ complexes with water, we mass selected the complex of interest with the first quadrupole, reacted the complex with water in the second quadrupole, and mass analyzed the products with the third quadrupole. To ensure consistent experimental conditions, the Ar gas was bubbled through water at room temperature, and a constant pressure of 0.1 Pa was maintained in the collision cell (second quadrupole) over the course of the experiments. $[MFeCl]^+$ and $[MFeCl_2]^+$ were each mass selected for reaction, and the water uptake was monitored. The best uptake was observed when collision energies were set to 0−2 V.

III. Results and Discussion

A. Active Sites of the Biomolecule. Chemical reactivity calculations using the condensed FFs (Table 1) on a particular geometry of M in water, extracted from CPMD simulations, indicate that the O2 atom (see Figure 1C) with a f^{HOMO} value of 0.18 possesses a strong nucleophilic character. Our natural partial charge (NPA) analysis shows that this hydroxyl group oxygen (O2) has a larger partial negative charge than the ring oxygen (O5) and methoxy oxygen (O1) in aqueous solution (see Table 2). This analysis indicates that the hydroxyl group oxygen atoms of the carbohydrate have a better Lewis base reactivity than the ring oxygen and the methoxy oxygen atoms. This result is in agreement with our previous findings for M in the gas phase,[22] which showed hydroxyl O2, O3, and O4 atoms being reactive atoms toward Fe^{III}.

Our CPMD simulations of the carbohydrate in water (Figure 1C) show that a water molecule is coordinated to the O2 atom after 14 ps and stays coordinated for the rest of simulation (56 ps), in agreement with the Fukui analyses that predict this oxygen as the most reactive site of the carbohydrate toward a Lewis acid (see Table 1). These results show the significant impact of solvation in the interactions between Fe^{III} and M and suggest that theoretical models based on gas phase calculations might be suitable to properly describe the coordination of ligands to biomolecules in solution.

The coordination of the single water molecule to the O2 atom, electronic, and steric effects seem to decrease the reactivity of the O2 atom toward Fe^{III} in aqueous solution. CPMD simulations of the carbohydrate and one Fe^{III} in water (Figure 1B) show that the Fe^{III}, initially coordinated octahedrally to six water molecules, coordinates to the O3 and O4 hydroxyl atoms within 27 ps and stays coordinated to these two hydroxyl oxygen atoms for the rest of the simulation (43 ps). According to our CPMD simulations, two water molecules bind to the carbohydrate-coordinated Fe^{III} within 31 ps, with the carbohydrate and water oxygens forming a square planar-like arrangement about the Fe^{III} ion. This shows that a single Fe^{III} ion interacts with two types of ligands; carbohydrate hydroxyl groups (O3 and O4) and water molecules. Furthermore, the partial negative charge (according to our NPA analysis) of the O3 atom is slightly smaller when Fe^{III} is present (see Table 2). The distances between Fe^{III} and O3 and O4 atoms are 3.1 ± 0.1 Å and 4.0 ± 0.1 Å, respectively, indicating that the metal ion is closer to the O3 atom than the O4 atom. Our NPA results support this finding and indicate a smaller negative charge for O3 than for O4 (Table 2). This effect is a result of Fe^{III} coordination. A comparison to our previously reported results for the gas phase[22] shows that the Fe^{III} and O3 and O4 distances are slightly larger (about 10%) in water than in the gas phase, which may be due to coordination of additional water molecules to Fe^{III}. The calculated binding energy[22] for Fe^{III} coordination to the biomolecule is $-98.7\ kJ\ mol^{-1}$, indicating that the complexation with a single Fe^{III} is favorable.

In comparison to our recent study of MFe^{III} in the gas phase,[22] we find that the presence of water impacts the coordination of the Fe^{III}. Our gas phase studies showed a coordination of the metal ion to O2, O3, and O4 atoms, but our present solution phase CPMD simulations show that the metal ion is coordinated to O3 and O4, but not to O2. In addition, it is found that a water molecule is coordinated to O2 instead, with an intermolecular hydrogen bond distance of 2.8 ± 0.2 Å (Figure 1C and Table 2). Results regarding inter- and intramolecular hydrogen

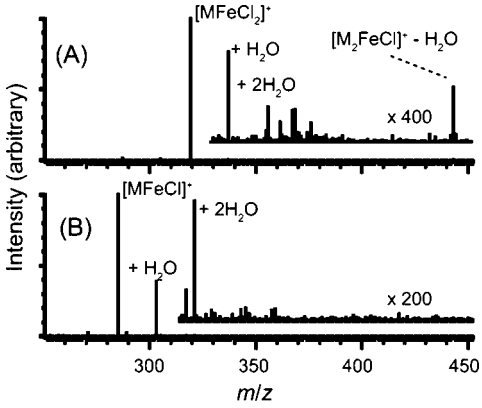

Figure 2. ESI mass spectra obtained by selecting (a) $[MFeCl_2]^+$ and (b) $[MFeCl]^+$ and colliding with water seeded in Ar. The spectra were collected with identical seeding and collision conditions, and the collision voltage was set to 1 V. The magnified portion of (a) reveals some contributions from the dimer dication. See text for details.

bonding interactions are discussed below. Our CMD simulations (Figure 1B) do not seem to detect coordination between M and Fe^{III}.

Our guided ion beam hydration experiments provide details of the coordination about the metal ion. Figure 2A,B offers a comparison of the water uptake for $[MFeCl_2]^+$ and $[MFeCl]^+$, respectively. $[MFeCl]^+$ readily picks up one water molecule, so that a strong peak at 303 *m/z* follows the parent peak at 285 *m/z*. Upon magnification (Figure 2B inset), a weak peak at 321 *m/z* can be seen, indicating the addition of a second water molecule. When $[MFeCl_2]^+$ is selected, the weak peak at 337 *m/z* (following the parent at 319 *m/z*) can only be seen with significant (x400) magnification. The *m/z* 337 peak, corresponding to the addition of a second water molecule (355 *m/z*), is barely distinguishable above the noise level. The data show that under the same conditions $[MFeCl]^+$ readily picks up one water molecule and $[MFeCl_2]^+$ does not.

The spectra obtained when $[MFeCl_2]^+$ is selected show evidence for appreciable contributions from $[(MFeCl_2)_2]^{2+}$. Specifically, peaks corresponding to two CH_3OH losses with two and three HCl losses from the dimer dication were identified. In addition, a peak corresponding to $FeCl_3$ and HCl loss was observed; we previously identified this species as a prominent fragment from $[M_2FeCl]^+$.[22] Interestingly, Zhan et al. similarly found that peaks initially attributed to singly charged monomers were discovered upon adduction with water to include significant contributions from doubly charged dimers.[46]

Despite the presence of the heavier complexes, we are confident in our assignment of water pick-up on the monomers. As the collision gas line was purged of water (with Ar), the contribution from the peaks assigned to water pick-up diminished in intensity. This was particularly obvious when monitoring the intense peak at 303 *m/z* ($[MFeCl]^+ + H_2O$). When $[MFeCl_2]^+$ was selected, the spectrum changed less dramatically with drier collision gas, which we explain in terms of weak initial pick-up of water. In summary, we are confident in attributing the peak at 303 *m/z* to $[MFeCl]^+ + H_2O$ because the intensity of the peak is strongly correlated to the seeding of water in the collision gas.

Because these experiments find that $[MFeCl]^+$ picks up one water molecule easily and $[MFeCl_2]^+$ does not, the data indicate that both monomer ions are tetracoordinate iron complexes comprising Cl and oxygen atoms. These data, which apply to liquid-phase structures, and the literature describing iron coordination compounds in the solid state do not support alternate conclusions.

The mass accuracy of the instrumentation and simple peak profiles observed of the reactant and product molecular ions indicate that the ionization mechanism does not involve proton transfer; for example, the *m/z* 337 peak does not arise from $[Fe^{II}Cl_2] + H^+$. Therefore, our experiments have studied $[Fe^{II}Cl]^+$ and $[Fe^{III}Cl_2]^+$, which manifest iron in +2 and +3 oxidation states, respectively (Melnik, M.; Ondrejkovicova, I.; Vancova, V.; Holloway, C.E. *Rev. Inorg. Chem.* **1997**, *17*, 55−286), have reviewed the crystallographic structures and optical spectra of nearly 900 monomeric iron coordination compounds of which ∼100 are examples of Fe^{II} and Fe^{III} compounds coordinated with one of more organic oxygen-containing ligands or water. Where necessary, chloride anions complete the coordination shell. The Fe^{II} complexes exhibit coordination numbers, *n*, of four and six. The Fe^{III} complexes exhibit coordination numbers with oxygen-containing ligands of $n = 4$, 5, 6, 7, and 8; structures with $n = 4$ and $n = 6$ are the most prevalent. On the basis of these solid state structures, we may expect $[MFeCl]^+$ to uptake one H_2O molecule to complete its tetracoordinate shell; uptake of two or more H_2O molecules would provide evidence for octahedral coordination. We may expect $[Fe^{III}Cl_2]^+$ to uptake two H_2O molecules during guided ion beam experiments if it forms an octahedrally coordinated molecular ion. Alternately, if $[Fe^{III}Cl_2]^+$ maintains a tetracoordinate structure, no water uptake would be observed.

Turning our attention to the liquid phase results, the tendency of $[MFeCl]^+$ to pick up water more efficiently than $[MFeCl_2]^+$ may be understood by considering the tetra-coordination motif suggested by our CPMD simulations. The simulations suggest that an ionic iron atom coordinates to two sites on M and two water molecules. Assuming that this motif applies, $[MFeCl_2]^+$ has a fully coordinated iron center, while $[MFeCl]^+$ requires one additional ligand to completely saturate the iron center. Therefore, $[MFeCl]^+$ can form a chemical bond with one water molecule, while $[MFeCl_2]^+$ cannot. The less intense peaks ($[MFeCl_2]^+$ with one or two water molecules and $[MFeCl]^+$ with two water molecules) require water addition via hydrogen bonding, and so the interaction, and therefore the peak intensity, is weaker.

The interpretations of previous CID results regarding tetracoordination at the Fe^{III} center are also consistent with our CPMD simulations. Carlesso et al.,[47] when discussing $[M_nFe]^{2+}$ complexes (where their M is mannose, whereas we considered[22] both mannose and methyl-α-D-mannopyrannoside), considered hexacoordinate iron centers. Their CID results show that M loss is common from complexes with $n \geq 3$, whereas sequential H_2O losses were observed with $n \leq 2$.[47] Our previous CID results also found that M loss occurred from $[M_2FeCl]^+$, but not from $[MFeCl]^+$.[22] In terms of the bonding motif indicated by our simulations, it seems that M loss does not occur when the coordination number around Fe is ≤4, suggesting that the Fe−M bonds are stronger when a tetracoordinate (or less) configuration is attained.

To study the coordination of more than one Fe^{III} to M, we performed chemical reactivity index calculations in the vicinity of Fe^{III} and water molecules and simulated M in water with two Fe^{III} ions (Figure 1D). The chemical reactivity calculations on a trajectory of MFe^{III} with the first shell of water molecules obtained from CPMD simulations show that the carbohydrate heavy atoms are not reactive toward a second Fe^{III} ion (Table 1). This finding is consistent with current and previous experimental results.[22,47] CPMD simulations show that the first

Fe^{III} is still coordinated to O3 and O4 atoms in the presence of a second Fe^{III}; however, the distance between Fe^{III} and O3 and O4 atoms is slightly larger in the presence of a second Fe^{III}, with values of 3.4 ± 0.1 Å and 4.3 ± 0.2 Å, respectively (Figure 1D and Table 2). Furthermore, the simulations with only one Fe^{III} show the metal ion almost symmetrically placed between the O3 and the O4 atoms with an angle of $54.4 \pm 12°$. With a second Fe^{III}, this angle becomes $44.2 \pm 9.7°$, and the Fe^{III} attached to M is coordinated to three water molecules instead of two. The second Fe^{III} prefers to be arranged with six water molecules in an octahedral symmetry in the second solvation shell. The closest distance between the first and the second Fe^{III} ions is 10.2 Å. We also note that the intermolecular hydrogen bond distance between the O2 and the coordinated water molecule increases to 3.25 ± 0.24 Å in the presence of the second Fe^{III} ion. In agreement with our studies in the gas phase,[22] we find that the presence of a second Fe^{III} ion increases the distances between the coordinated Fe^{III} ions and the O3 and O4 atoms of the carbohydrate. The coordination of the second Fe^{III} to the biomolecule in the gas phase is possible,[22] whereas the inclusion of explicit solvent molecules shows that the presence of water impacts the coordination chemistry since the second Fe^{III} ion bonds to water molecules rather than to the carbohydrate (see above).

Our NPA analysis (including all solute and solvent molecules) indicates that the partial positive charge on the first Fe^{III} increases from 0.7 to 1.4 in the presence of the second Fe^{III} (Table 2). This finding is consistent with our simulations, since the distances of the coordinated ligands to the carbohydrate-coordinated Fe^{III} are larger when a second Fe^{III} is present in the system, indicating less electron donation capability for the carbohydrate-coordinated Fe^{III}.

The present first principles results are in agreement with experiments, which show only one Fe^{III} coordinated to the carbohydrate in solution.[22,47] In contrast to experiment and ab initio simulations, our CMD simulations show that both Fe^{III} ions form complexes only with water molecules and do not coordinate to the biomolecule. These discrepancies can be attributed to the quality of the force field parameters for the metal ion, usage of fixed partial charge parameters for the different hydroxyl oxygens in the carbohydrate (neglecting of charge polarization), failure to distinguish between equatorial and axial orientations of the carbohydrate hydroxyl groups, and ignoring the conformation dependence of steric effects in our CMD simulations.

B. Glycosidic Linkage Flexibility. The relative torsional energies of the glycosidic linkage (φ) of M (see Figure 1A and Methods) were studied using CPMD and CMD simulations in water. Changes arising in PMF as a function of torsional angle derived from these calculations are presented in Figure 3. Figure 3A shows the calculated PMF values of the glycosidic linkage for M, MFe^{III}, and MFe^{III}_2 based on CPMD simulations (see Methods and refs 6, 7, and 22 for details). Different trends for the conformational preference of the glycosidic linkage of M are observed by CPMD simulations: the $g+ > t > g-$ trend observed in the free M becomes $g+ > g- > t$ and the minimum shifts from 60° to 70° upon coordination of one Fe^{III} to M in water (Figure 2A). The presence of the second Fe^{III} does not influence the calculated thermodynamic trend for the glycosidic linkage conformation in the vicinity of a single Fe^{III} ion (Figure 3A), consistent with the fact that a second Fe^{III} does not coordinate to the MFe^{III} complex.

According to our CMD simulations, the trend obtained for the glycosidic linkage conformation $g+ > g- > t$ for the free

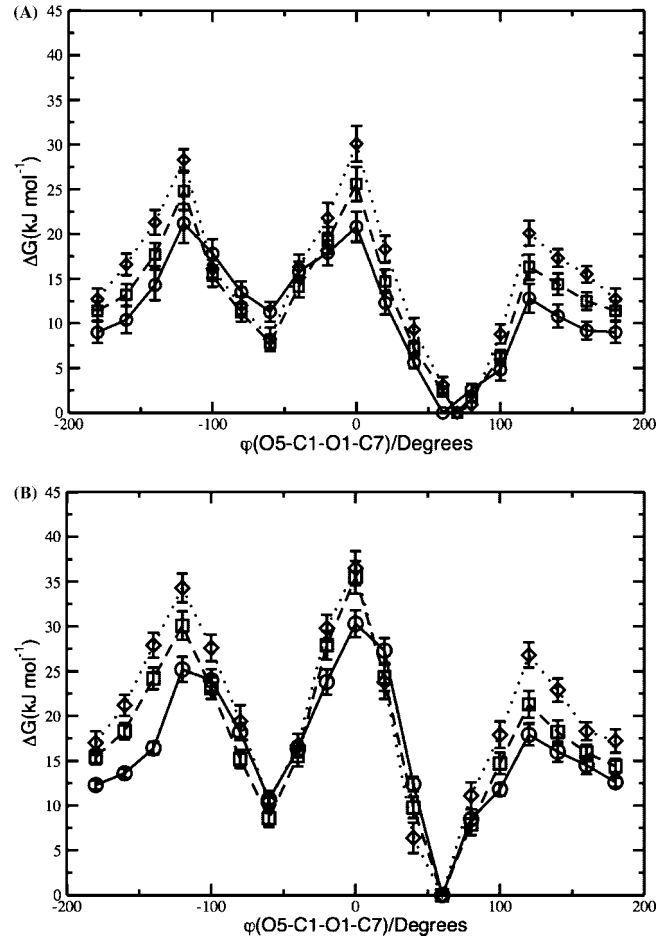

Figure 3. Calculated torsional energy change of the glycosidic linkage of methyl-α-D-mannopyranoside (solid line) and its energy change in the vicinity of one (dashed line) and two Fe^{III} ions (dotted line), with the potential of mean force method: (A) CPMD simulations, (B) CMD simulations. The inset plot (B) presents the calculated energy differences of the glycosidic linkage of methyl-α-D-mannopyranoside with the perturbation and potential of mean force methods by CMD simulations. Errors were calculated using the time-dependent standard deviation method.

carbohydrate is retained in aqueous solution in the presence of the Fe^{III} ions, which are coordinated to water molecules rather than to the biomolecule (see Figure 3B). Furthermore, in stark contrast to the CPMD results, our CMD simulations do not indicate a significant shift of the minimum energy torsional angle of the glycosidic linkage and predict +60° as the minimum for M, MFe^{III}, and MFe^{III}_2 in water. For the gas phase, this trend is $g+ > t \approx g-$ as reported previously[22] and indicates that water stabilizes the $g-$ orientation of the glycosidic linkage over its t orientation upon coordination of Fe^{III}.

C. Hydrogen Bonding Properties. According to our CPMD simulations, the average intramolecular hydrogen bonding distances between O2−O3, O3−O4, and O4−O6 (Figure 1) of M in water vary between 2.1 and 4.5 Å. In contrast, CMD simulations predict that these intramolecular distances are between 2.4 and 3.7 Å. The intramolecular hydrogen bonds between the O2 and the H attached to O3 are shorter than those for O3−O4 and O4−O6 according to our CPMD simulations (Table 3). Furthermore, the predicted intermolecular hydrogen bonds between O2−water, O3−water, and O4−water indicate a stronger coordination of the O2 atom to a water molecule (as compared to the O3-water and O4-water hydrogen bonds) via the shorter O2−water distance (see Table 3). This finding is in

TABLE 3: Specific Bond Lengths and Bond Angles of Methyl-α-D-mannopyranoside and Its Complexes with Fe^{III} Ions in Water Calculated via CPMD and CMD Simulations[a]

	M		M:Fe^{III}		M:Fe^{III}_2	
	CPMD	**CMD**	**CPMD**	**CMD**	**CPMD**	**CMD**
O3−H2/Å	2.1 ± 0.3	2.4 ± 0.5	2.1 ± 0.2	2.4 ± 0.4	2.2 ± 0.1	2.5 ± 0.4
O4−H3/Å	2.5 ± 0.4	2.6 ± 0.6	3.0 ± 0.3	2.7 ± 0.5	3.1 ± 0.3	2.8 ± 0.4
O2−O_{water}/Å	2.8 ± 0.3	3.1 ± 0.3	2.9 ± 0.2	2.9 ± 0.5	3.2 ± 0.2	2.9 ± 0.3
O3−O_{water}/Å	3.4 ± 0.2	2.9 ± 0.5	4.8 ± 0.3	3.0 ± 0.4	5.1 ± 0.4	3.1 ± 0.4
O4−O_{water}/Å	3.8 ± 0.3	3.2 ± 0.4	5.0 ± 0.5	3.1 ± 0.5	5.2 ± 0.4	3.2 ± 0.4
O6−H4/Å	4.5 ± 0.4	3.6 ± 0.9	2.5 ± 0.4	3.3 ± 0.6	2.6 ± 0.3	3.5 ± 0.7
θ(O2H2O3)/Degrees	127.9 ± 8.0	105.2 ± 22.8	130.7 ± 4.5	107.7 ± 19.8	128.8 ± 5.3	109.9 ± 13.5
θ(O3H3O4)/Degrees	115.3 ± 11.4	103.7 ± 25.4	117.7 ± 5.6	105.2 ± 20.2	113.6 ± 4.9	113.3 ± 18.4
θ(O4H4O6)/Degrees	123.5 ± 12.3	107.8 ± 22.5	124.6 ± 7.3	106.9 ± 19.9	122.1 ± 8.2	108.0 ± 16.2
Fe_I-O3/Å			3.1 ± 0.2	>5.5	3.4 ± 0.1	>5.5
Fe_I-O4/Å			4.0 ± 0.2	>6.1	4.4 ± 0.2	>6.3
Fe_I-O_{water1}/Å			2.1 ± 0.2		2.0 ± 0.3	
Fe_I-O_{water2}/Å			2.2 ± 0.1		2.3 ± 0.1	
θ(O3FeO4)/Degrees			54.4 ± 12.0		44.2 ± 9.7	
Fe_{II}-O_{water}/Å					2.2 ± 0.3	

[a] Atom numbers listed here are illustrated in Figures 1C and 1D: methyl-α-D-mannopyranoside, methyl-α-D-mannopyranoside and one Fe^{III} ion, and methyl-α-D-mannopyranoside and two Fe^{III} ions in water.

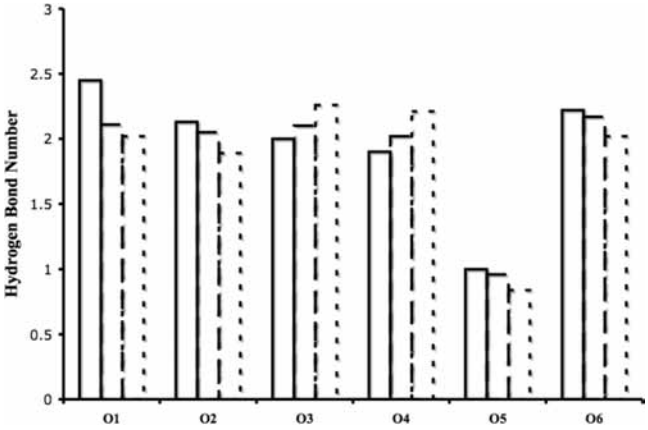

Figure 4. Average numbers of hydrogen bonds between specific methyl-α-mannopyranoside oxygens and water molecules for the (—) *g*+, (- - -) *t*, and (•••) *g*− orientations of the glycosidic linkage of methyl-α-mannopyranoside via CPMD simulations at room temperature.

agreement with our chemical reactivity calculations, which identify the O2 atom as the most reactive carbohydrate hydroxyl oxygen toward ligands. Our CPMD simulations show that the water ligand tends to coordinate to O2 rather than to O3 or O4. Our CMD simulations do not show a significant difference in intermolecular hydrogen bond distances for these hydroxyl oxygen atoms in water. In addition, a comparison to results obtained for the gas phase,[22] indicates that intermolecular hydrogen bonds between the biomolecule and solvent molecules increases the intramolecular hydrogen bond distances between O2−O3, O3−O4, and O4−O6 (Figure 1) by values varying between 0.4 and 1.7 Å.

Figure 4 shows the average number of hydrogen bonds between the carbohydrate and surrounding water molecules obtained from three distinct CPMD simulations for the *g*+, *g*−, and *t* orientations of the glycosidic linkage (each simulation was performed for 60 ps). For these analyses, following the work of Parrinello and Molteni[48] and our previous studies,[6,7,22] the criteria for the existence of a hydrogen bond were defined as $O_D-H \leq 1.5$ Å and $H-O_A \leq 2.4$ Å, where O_D and O_A represent donor and acceptor oxygen atoms, respectively. The angular criterion was set to values larger than 120°. According to our analyses, the total number of intermolecular hydrogen bonds is highest for the *g*+ conformation, while the *t* conformation exhibits a slightly larger number than for the *g*− orientation. In agreement with our previous studies, the hydrogen bond capacity of the carbohydrate atoms in water is not satisfied since each hydroxyl group may participate in three hydrogen bonds (one donor and two acceptors), while O5 (Figure 1C) may participate in two hydrogen bonds as an acceptor.

CPMD simulations and a comparison to our previous results in the gas phase[22] indicate that the presence of a single Fe^{III} ion weakens the intramolecular hydrogen bonds between the O3 and the O4 atoms since these hydroxyl group oxygens are coordinated to the metal ion (see Table 3). The average O4−O6 intramolecular hydrogen bond distance becomes shorter in comparison with those obtained for the aqueous carbohydrate without a metal ion (Table 3). This result indicates that the intramolecular hydrogen bonds between these hydroxyl groups become stronger, due to the coordination of Fe^{III} to O3 and O4. In addition, we find that two water molecules are coordinated to the carbohydrate-coordinated Fe^{III} ion with average Fe−water oxygen distances of 2.1 ± 0.2 Å and 2.2 ± 0.1 Å. In contrast, our CMD simulations predict intramolecular H bonds between O2 and O3, and O3 and O4 in the presence of Fe^{III} (Table 3). The hydroxyl oxygen atoms are also coordinated to water molecules with average intermolecular H-bond distances varying between 2.7 Å and 3.5 Å.

According to our CPMD simulations, the presence of the second Fe^{III} ion does not impact the number of intramolecular and intermolecular H bonds of the carbohydrate. However, we find that both intramolecular and intermolecular H-bond distances are slightly larger in comparison with those calculated for the H bonds in the vicinity of a single Fe^{III} ion (Table 3). Instead of only two water molecules, three water molecules are coordinated to the carbohydrate-coordinated Fe^{III} ion (Figure 1D). This arrangement might be due to the larger distances between the Fe^{III} and the O3 and O4 atoms of the carbohydrate (see above); since it may allow electron donation from more than two water ligands, as shown by our NPA results (Table 2). Furthermore, a comparison to our recent studies in the gas phase shows that the presence of intermolecular hydrogen bonds between solvent molecules and the carbohydrate affects the number of intramolecular hydrogen bonds in the gas phase upon Fe^{III} coordination; no intramolecular hydrogen bonds were obtained between O2−O3 upon Fe^{III} coordination in the gas

phase. In contrast, intramolecular hydrogen bonds between O2−O3 do exist in water upon coordination of Fe^{III}.

The average distance between the second Fe^{III} and its six coordinated water oxygen atoms is 2.2 ± 0.3 Å, in accord with our recent studies[22] and with diffraction spectroscopy measurements for hydrated Fe^{III} ion.[38] The first shell coordination number was found to be six in all cases for the second Fe^{III} ion, indicating that the interaction between the Fe^{III} and the biomolecule does impact the coordination number of water molecules reported for a hydrated Fe^{III} ion. In contrast, the CMD simulations suggest that both Fe^{III} ions are coordinated to water molecules and not to the biomolecule.

Overall, the treatment of quantum effects by CPMD simulations provides a different picture of the interaction between Fe^{III} and the saccharide methyl-α-mannopyranoside when compared to the results of our CMD simulations. Differences obtained between CPMD and CMD simulations may indicate that better force field parameters for aqueous Fe^{III} and carbohydrates are needed. Differences in determined structures might have an impact on the determined chemical reactivity of the biomolecule toward metal ions. We also note that simulated intra- and intermolecular H bonds differ from each other via CPMD and CMD simulations. This result is in agreement with our recent theoretical studies.[6,7,22] We find that the presence of water molecules affects the chemical reactivity, coordination chemistry, structural and thermodynamic properties of biometallic complexes and thus, calls for care when one attempts to predict the chemical properties of biometallic complexes in solution from the results of gas-phase calculations.

IV. Conclusion

We have used an integrated approach based on theoretical calculations, molecular simulations, and mass spectrometric measurements to study the active sites of a biomolecule toward metal ions in aqueous solution. Results were compared to those obtained via classical MD simulations. The insights obtained from CPMD simulations are consistent with the chemical reactivity calculations, natural partial charge analysis, and mass spectrometric measurements.

Our first principles studies indicate, in agreement with experiment, that only one Fe^{III} ion coordinates to M in water. Theoretical calculations and CPMD simulations show that a water molecule coordinates to one of the hydroxyl groups (O2 atom) of M. Our CPMD simulations further indicate that two hydroxyl oxygen atoms of the saccharide and two water molecules are coordinated to a single Fe^{III} ion in a square planar-like arrangement, whereas a second Fe^{III} ion resides in the second solvation shell and coordinates to six water molecules in octahedral geometry. These findings are in accord with our mass spectrometric results, and our structural parameters for the second Fe^{III} agree with neutron diffraction data and recent theoretical calculations[38] for $Fe(H_2O)_6^{3+}$. Our CMD simulations provide no clear coordination of Fe^{III} to the carbohydrate, instead indicating that both Fe^{III} ions interact only with surrounding water molecules.

According to our CPMD simulations, coordination of a metal ion affects the preferred glycosidic linkage orientation of the carbohydrate. The glycosidic linkage preference changes from $g+ > t > g-$ to $g+ > g- > t$ upon coordination to Fe^{III} in aqueous solution. CPMD simulations clearly indicate that the preference of the conformation of the carbohydrate and coordination of the metal ion is influenced by intra- and intermolecular hydrogen bonds. Our results further demonstrate that CMD simulations are insensitive to these effects and suggest a need for better force field parameters for aqueous Fe^{III} and carbohydrate.

This study illustrates that chemical reactivity calculations, CPMD simulations, and mass spectrometric measurements can provide important insights into the structure and function of biometallic complexes in solution and supports our studies for biometallic compounds in the gas phase. Furthermore, we show that the solution environment impacts the active sites of a biomolecule toward ligands. Currently, we are studying the coordination of divalent and trivalent metal ions to amino acids, peptides, and proteins in the gas phase and in aqueous solution. We are confident that validated first principles approaches in different phases (gas and solution) will help to predict unknown reaction mechanisms of important physiological processes-such as receptor and ligand interactions and protein mis-folding in the presence of metal ions-that are crucial to drug design, medicine, biochemistry, and nanobiotechnology.

Acknowledgment. The authors thank T. C. Allison and Y. Simon-Manso for helpful discussions. D.B. thanks the National Research Council of the National Academy of Sciences for a postdoctoral fellowship.

References and Notes

(1) Coskuner, O.; Deiters, U. K. *Z. Phys. Chem.* **2006**, *220*, 349.
(2) Coskuner, O.; Deiters, U. K. *Z. Phys. Chem.* **2007**, *221*, 785.
(3) Stigter, D.; Alonso, D. O.; Dill, K. A. *Proc. Natl. Acad. Sci. U.S.A.* **1991**, *88* (10), 4176.
(4) Wolfenden, R.; Radzicka, A. *Science* **1994**, *265* (5174), 936.
(5) Kirschner, K. N.; Woods, R. J. *Proc. Natl. Acad. Sci. U.S.A.* **2001**, *98* (19), 10541.
(6) Coskuner, O. *J. Chem. Phys.* **2007**, *127*, 015101.
(7) Coskuner, O.; Bergeron, D. E.; Rincon, L.; Hudgens, J. W.; Gonzalez, C. A. *J. Chem. Phys*. 2008, *129*, 045102.
(8) Qin, S.; Zhou, H.-X. *Biopolymers* **2007**, *86* (2), 112.
(9) Jung, A.; Berlin, P.; Wolters, B. *IEE Proc.-Nanbiotechnol.* **2004**, *151* (3), 87.
(10) Ohtaki, H.; Radnai, T. *Chem. Rev. (Washington D.C.)* **1993**, *93*, 1157.
(11) Thanki, N.; Thornton, J. M.; Goodfellow, J. M. *J. Mol. Biol.* **1988**, *202*, 637.
(12) Rossky, P.; Karplus, M. *J. Am. Chem. Soc.* **1979**, *101*, 1913.
(13) Vank, J. C.; Zamora, M. A.; Csizmadia, I. G.; Baldoni, H. A.; Rodrigues, A. M.; Enriz, R. D.; Sosa, C. P.; Perczel, A.; Kucasman, A.; Farkas, O.; Deretey, E. *Can. J. Chem.* **2002**, *80* (7), 832.
(14) Silanpaa, A. J.; Aksela, R.; Laasonen, K. *Phys. Chem. Chem. Phys.* **2003**, *5*, 3382.
(15) Tunega, D.; Haberhauer, G.; Gerzabek, M.; Lischka, H. *J. Phys. Chem. A* **2000**, *104*, 6824.
(16) Coskuner, O.; Jarvis, E. A. A. *J. Phys. Chem. A* **2008**, *112* (12), 2628.
(17) Wako, H. *J. Protein Chem.* **1989**, *8* (6), 733.
(18) Woo, H-J.; Dinner, A. R.; Roux, B. *J. Chem. Phys.* **2004**, *121*, 6392.
(19) Zuegg, J.; Gready, J. E. *Glycobiology* **2000**, *10* (10), 959.
(20) Calfisch, A.; Karplus, M. *Proc. Natl. Acad. Sci. U.S.A.* **1994**, *91* (5), 1746.
(21) Smolin, N.; Winter, R. *J. Phys. Chem. B* **2004**, *108* (40), 15928.
(22) Coskuner, O.; Bergeron, D. E.; Hudgens, J. W.; Rincon, L.; Gonzalez, C. A. *J. Phys. Chem. A* **2008**, *112* (13), 2940.
(23) Beyer, M. K. *Mass Spec. Rev.* **2007**, *26*, 517.
(24) Stace, A. J. *Phys. Chem. Chem. Phys.* **2001**, *3*, 1935.
(25) Stace, A. J. *J. Phys. Chem. A* **2002**, *106*, 7993.
(26) Castleman, A. W.; Bowen, K. H. *J. Phys. Chem.* **1996**, *100*, 12911.
(27) Jarrold, M. F. *Acc. Chem. Res.* **1999**, *32*, 360.
(28) Jarrold, M. F. *Annu. Rev. Phys. Chem.* **2000**, *51*, 179.
(29) Rodgers, M. T.; Armentrout, P. B. *Acc. Chem. Res.* **2004**, *37*, 989.
(30) Bylaska, E. J. de Jong, W. A. Kowalski, K. et al., *NWCHEM, A Computational Chemistry Package for Parallel Computers, Version 5.0*; Pacific Northwest National Laboratory: Richland, Washington 99352−0999, 2006.
(31) Certain commercial equipment and software are identified in this paper in order to specify the experimental procedure adequately. Such identification is not intended to imply recommendation or endorsement by the National Institute of Standards and Technology, nor is it intended to

imply that the software or equipment identified are necessarily the best available for the purpose.

(32) Troullier, N.; Martins, J. L. *Phys. Rev. B* **1991**, *43*, 1993.

(33) (a) Lee, C.; Yang, W.; Parr, R. C. *Phys. Rev. B* **1988**, *37*, 785. (b) Ramalho, T. C.; Taft, C. A. *J. Chem. Pys.* **2005**, *123*, 054319. (c) Leung, K.; Rempe, S. *Phys. Chem. Chem. Phys.* **2006**, *8*, 2153. (d) Ramaniah, L. M.; Bernasconi, M.; Parrinello, M. *J. Chem. Phys.* **1999**, *111*, 1587. (e) Raguei, S.; Klein, M. L. *J. Chem. Phys.* **2002**, *116*, 196. (f) Soper, A. K. *Chem. Phys.* **2000**, *258*, 1. (g) Neuefeind, J.; Benmore, C. J.; Tomberlini, B.; Egelstaff, P. A. *J. Phys.: Condens. Matter* **2002**, *14*, L249. (h) Hura, G.; Sorenson, J. M.; Glaeser, R. M.; Head-Gordon, T. *J. Chem. Phys.* **2000**, *113*, 9140. (i) Sorenson, J. M.; Hura, G.; Glaeser, R. M.; Head-Gordon, T. *J. Chem. Phys.* **2000**, *113*, 9149. (j) Head-Gordon, T.; Hura, G. *Chem. Rev.* **2002**, *102*, 2651. (k) Tomberlini, B.; Benmore, C. J.; Egelstaff, P. A.; Neuefield, J.; Honkimaki, V. *J. Phys.: Condens. Matter* **2000**, *12*, 2597. (l) Chen, B.; Ivanov, I.; Klein, M. L.; Parrinello, M. *Phys. Rev. Lett.* **2003**, *91*, 215503–1. (m) Hart, R. T.; Mei, Q.; Benmore, C. J.; Neuefeind, J. C.; Turner, J. F. C.; Dolgos, M.; Tomberlini, B.; Egelstaff, P. A. *J. Chem. Phys.* **2006**, *124*, 134505. (n) Hart, R. T.; Benmore, C. J.; Neuefeind, J.; Kohara, S.; Toberlini, B.; Egelstaff, P. A. *Phys. Rev. Lett.* **2005**, *94*, 047801.

(34) Allen, M. P.; Tildesley, D. *Computer Simulations of Liquids*; Oxford University Press: New York, 1987.

(35) Kale, L.; Skeel, R.; Bhandarkar, M.; Brunner, R.; Gursoy, A.; Krawetz, N.; Philips, J.; Shinozaki, A.; Varandarajan, K.; Schulten, K. *J. Comput. Phys.* **1999**, *151*, 283.

(36) Damm, W.; Frontera, A.; Tirado-Rives, J.; Jorgensen, W. L. *J. Comput. Chem.* **1997**, *18*, 1955.

(37) Rappe, A. K.; Casewit, C. J.; Colwell, K. S.; Goddard III, W. A.; Skiff, W. M. *J. Am. Chem. Soc.* **1992**, *114*, 10024.

(38) (a) Coskuner, O.; Jarvis, E. A. A.; Allison, T. C. *Angew. Chem.* **2007**, *119* (41), 7999. (b) Coskuner, O.; Jarvis, E. A. A.; Allison, T. C. *Angew. Chem., Int. Ed.* **2007**, *46* (41), 7853.

(39) (a) Parr, R.; Yang, W. *Density Functional Theory of Atoms and Molecules*; Oxford University Press: New York, 1989. (b) Parr, R.; Yang, W. *J. Am. Chem. Soc.* **1984**, *106*, 4049. (c) Yang, W.; Parr, R.; Pucci, R. *J. Chem. Phys.* **1984**, *81*, 2682. (d) Yang, W.; Parr, R. G. *Proc. Natl. Acad. Sci. U.S.A.* **1985**, *82*, 6723.

(40) Cioloski, J.; Martinov, M.; Mixon, S. T. *J. Phys. Chem.* **1993**, *97*, 10948.

(41) Senet, P. J. *J. Chem. Phys.* **1997**, *107*, 2516.

(42) Contreras, R. R.; Fuentealba, P.; Galvan, M.; Perez, P. *Chem. Phys. Lett.* **1999**, *304*, 405.

(43) See, for example, (a) Fuentealba, P.; Contreras, R. R. *Reviews of Modern Chemistry. A Cellebration of the Contribution of Robert G Parr*; World Scientific: Singapore, 2002; p 1013. (b) Chermette, H.; Boulet, P.; Portmann, S.; *Reviews of Modern Quantum Chemistry. A Cellebration of the Contribution of Robert G Parr*; World Scientific: Singapore, 2002; p 992. (c) Fuentealba, P.; Perez, P.; Contreras, R. R. *J. Chem. Phys.* **2000**, *113*, 2544. (d) Bullat, F. A.; Chamorro, E.; Fuentealba, P.; Torro-Labbe, A. *J. Phys. Chem. A* **2004**, 108–342.

(44) Frisch, M. J. Trucks, G. W. Schlegel, H. B. Scuseria, G. E. Robb, M. A. Cheeseman, J. R. Montgomery, J. J. A. Vreven, T. Kudin, K. N. Burant, J. C. Millam, J. M. Iyengar, S. S. Tomasi, J. Barone, V. Menucci, B. Cossi, M. Scalmani, G. Rega, N. Petterson, G. A. Nakatsuji, H. Hada, M. Ehara, M. Toyota, K. Fukuda, R. Hasegawa, J. Ishida, M. nakajima, T. Honda, Y. Kitao, O. Nakai, H. Klene, M. Li, X. Knox, J. E. Hratchian, H. P. Cross, J. B. Bakken, V. Adamo, C. Jaramillo, J. Gomperts, R. Straatmann, R. E. Yazyev, O. Austin, A. J. Cammi, R. Pomelli, C. Ochterski, J. W. Ayala, P. Y. Morkuma, K. Voth, G. A. Salvador, P. Dannenberg, J. J. Zakrzweski, V. G. Dapprich, S. Daniels, A. D. Strain, M. C. Farkas, O. Malick, D. K. Rabuck, A. D. Raghavachari, K. Foresman, J. B. Ortiz, J. V. Cui, Q. Baboul, A. G. Clifford, S. Ciolowski, J. Stefanov, B. B. Liu, G. Liashenko, A. Piskorz, P. Komaromi, I. Martin, R. L. Fox, D. J. Keith, T. Al-Laham, M. A. Peng, C. Y. Nanayakkara, A. Challacombe, M. Gill, P. M. W. Johnson, B. Chen, W. Wong, M. W. Gonzalez, C.; Pople, J. A. *Gaussian 03, Revision C.02*; Gaussian, Inc: Wallingford, CT, 2004.

(45) (a) Perdew, J. P.; Burke, K.; Ernzerhof, M. *Phys. Rev. Lett.* **1996**, *77*, 3865. (b) Perdew, J. P.; Burke, K.; Ernzerhof, M. *Phys. Rev. Lett.* **1997**, *78*, 1396.

(46) Zhan, D. L.; Rosell, J.; Fenn, J. B. *J. Am. Soc. Mass Spec.* **1998**, *9*, 1241.

(47) Carlesso, V.; Afonso, C.; Fournier, F.; Tabet, J. C. *Int. J. Mass Spec.* **2002**, *219*, 559.

(48) Molteni, C.; Parrinello, M. *J. Am. Chem. Soc.* **1998**, *120*, 2168.

JP805747F